Radio Channel Characterization of Mid-Band 5G Service Delivery for Ultra-Low Altitude Aerial Base Stations

PHILIP A. CATHERWOOD[1], (Member, IEEE), **BRENDAN BLACK**[1],
EBRAHIM BEDEER MOHAMED[1], (Member, IEEE), **ADNAN AHMAD CHEEMA**[1],
JOSEPH RAFFERTY[2], (Member, IEEE), AND **JAMES A. D. MCLAUGHLIN**[1]

[1]School of Engineering, Ulster University, Jordanstown Campus, Newtownabbey BT370QB, U.K.
[2]School of Computing and Mathematics, Ulster University, Jordanstown Campus, Newtownabbey BT370QB, U.K.

Corresponding author: Philip A. Catherwood (p.catherwood@ulster.ac.uk)

ABSTRACT This paper presents a study which evaluated the potential for using ultra-low altitude, unmanned aerial vehicles to deliver fifth-generation (5G) cellular connectivity, particularly into areas requiring short-term enhancement in coverage. Such short-term enhancement requirements may include large gatherings of people or during disaster scenarios where there may be service outages or a need for increased bandwidth. An evaluation of this approach was conducted with empirically generated results regarding signal quality and cellular coverage—illustrating the potential of using unmanned ultra-low altitude aerial vehicles to deliver 5G cellular mobile services. Specifically, channel gain, mean time delay of the received signals (τ_{mean}), and the root-mean-square spread of the delay (τ_{rms}) were investigated for two distinct user modes at three different drone heights for three selected environments—an open area (field), a tree-lined environment, and an enclosed area. Maximum likelihood estimates for the various drone heights, user modes, and operational environments were found to be Rician distributed for the received signal strength measurements, whereas τ_{mean} and τ_{rms} for the open and tree-lined environments were Weibull distributed with the enclosed area tests being lognormally distributed. The paper also investigates how the channel gain may be affected when operating in each of the various global bands allocated for mid-5G communications, namely, Europe, China, Japan, South Korea, and North America. These regional mid-5G band allocations were found to yield minimal variance for all the environments considered.

INDEX TERMS 5G, 5th generation, personalized networks, propagation, signal delay, signal reliability, UAV.

I. INTRODUCTION

Unmanned aerial vehicles (UAVs), often termed ''drones'', may have a key role to play in the emerging 5th Generation cellular mobile network (hereafter denoted as 5G). UAVs have the potential to act as temporary 5G network access points to local users when a need to extend or reinforce the local network arises. A unique advantage of drone-hosted base stations is that they possess the ability to alter their position and location to address migrating crowds, changing environments, and other service-limiting parameters. Such networks are expected to support several appropriate scenarios, including raising the quality of cellular coverage in rural areas [1], assisting first responders in various accident situations or disaster zones [2]–[4], facilitating rescue and relief operations [5], and supporting connectivity during cellular network overloads or power failure events [6]. These works serve to highlight the potential applications and impact such technology usage may have across a number of sectors. Additionally, they help to rationalize the need to explore the key aspects of the technology, such as the radio links necessary for successful and robust operation. Each of these scenarios are likely to require robust communication channels and may necessitate an increase in communication capacity.

The concept of UAV as a key component of a cellular network has been previously demonstrated by Gharibi *et al.* [7] as an Internet of Drones (IoD) cellular network topology

which uses the network to control the movements and communication of multiple drones. A similar premise was presented by Nokia [8] who developed an ultra-miniaturized 4G base station weighing only 2 Kg. The system was successfully tested on a commercial quadcopter to provide coverage over remote areas. While this work only addressed a single category of environmental scenario, it acts as an indicator of possible use cases. Naqvi et al. [9] reported upon an examination into how UAVs might satisfy higher data rates in a millimeter-wave 5G network across a range of heights from 10 m to 200 m and concluded that the use of UAVs in tandem with conventional cellular network can serve to improve the cellular system as well as reduce the time and financial investment required for network planning. This research highlighted the potential for using drones to satisfy changeable 5G network demand however the focus was on the higher frequency bands (28 GHz) and didn't address different user modes or a broad range of localized environments. Such papers do however indicate the opportunities and interest to deliver cellular connectivity in novel ways.

A number of studies have investigated the radio channel for drone-to-cellular base station links at 800 MHz [10], 850 MHz [11], and at 5 GHz [12], at dual bands 986 MHz and 5.06 GHz [13], as well as computer modeling of the channel at 850 MHz and 2.4 GHz [14]. Findings of [10] support the need for height-dependent descriptions of the air-to-ground propagation channel, however this work concentrated on heights of 100 m for horizontal drone-user separations of many kilometers which doesn't address the application of personalized very- and ultra-low altitude communications. While the application in [11] had a focus on drone management using the cellular network as opposed to providing robust cellular service to a ground-based user the radio channel between a drone and the ground is still under consideration for suburban environments. The campaign in [11] used a ground-based unit positioned on a base station structure of significant height and covered a large geographical area. However it offered important supporting work in describing the secondary signal hop from the local drone to the established communications network as any aerial drone is typically an intermediate node between user and an established wireless network. Research presented in [12] modeled a sizable number of inter-networked drones over a 2.6 Km^2 area with consideration given to a range of operational bandwidths; this is chiefly concerned with the large-scale deployment of aerial communication networks. It does help to generally inform the wider scenario of connecting many local drones to help establish a more robust backhaul to the established network. While this is essential for understanding future extensive networks, it does not suitably address the localized links upon which such a system is fundamentally reliant.

Investigations in [13] explored measurements and modeling for drone heights of 600 m and horizontal separations of up to 50 Km, presenting both path loss and τ_{RMS} values for a range of urban and suburban environments. For very large

areas it was found that τ_{RMS} values increased for more open spaces (typically due to increased absorption loss of multiple reflected signals by building); this result cannot be assumed to be directly applicable to the very low levels (VLL) short range links presented herein but does help to visualize scenarios where a user or group of users receive a service from a local drone as well as another more distant drone should the need arise. Theoretical path loss models in [14] depicted values for ground to drone links across a height range of 10 m to 1 Km. This model does not concentrate on user modes or a suitable range of environments that are essential to understand if the solution is to be widely deployed. Furthermore the focus of the work was on path loss with no signal time delay parameters explored. It does however indicate that the line of sight path loss changes by only small amounts for altitudes above 400 m and path loss values are dominated by free space attenuation. To this end, it is important in the work presented here to consider both path loss effects due to free space attenuation as well as the environmental loses (known as small-scale path loss) due to the VLL considered in the presented paper. In general, these activities offer interesting insights into how drone-to-cellular communication channels might perform for a number of frequencies, however they cannot be directly applied to the new 5G mid-band operating frequencies and bandwidths or to ultra-low altitude short range links.

Previously published research that has explicitly concentrated upon VLL airspace communications include the aforementioned [12] where the authors modeled drone to cell tower communications below 500 feet (150m) at 5 GHz. In addition, Shi et al. [15] presented channel measurements at 10, 20, and 30 m with an analysis of current 3/4G cellular and upper band Wi-Fi frequencies. Furthermore, Fotouhi et al. [16] focused on developing flight algorithms to improve the spectral efficiencies of migrating drones at a frequency of 2 GHz and at a drone height of 10 m [16]. The work in [15] analyzed a range of heights between 10-30 m for 900 MHz, 1800 MHz, and 5 GHz with a horizontal transmitter-receiver separation of between 10-100 m. The focus was on path loss only for a line of sight scenario and a forest area and did not explore the effects of user modes as it was not body-centric in nature and did not study the wideband signal delay parameters relating to the radio channel. While the focus of these VLL campaigns are different from the new research presented in this paper it does highlight the benefits of delivering cellular connectivity through aerial vehicles at heights just above the ground. Indeed such work serves to emphasize the potential for VLL communications and although [12] operates at 500 m which is above the legal restricted heights for the US [17] (with similar rules applying in other parts of the world), the studies described in [15] and [18] helps to inform use cases and clearly supports the need for reliable prediction of coverage of emerging air-to-ground wireless services, however neither have specifically addressed the new 5G cellular bands across a broad range of environments or for various cell phone user modes.

Network simulations presented by Fotouhi *et al.* [19] explore multiple aerial cellular base stations which are in continual motion; it was found that the constant movement increases the throughput and reduces the number of drones required. A drone in motion is thus a typical scenario in a deployment scenario and is thus considered. These previous characterization and modeling studies all focus upon understanding the channel gain (in most cases expressed as path loss) or data throughput; the authors have not discovered any relevant works that specifically address the delay statistics for mid-band 5G drone to cell phone user arrangements or furthermore to make a comparison between the allocated global radio bands.

Other practical challenges to deployment of aerial cellular 5G networks include the restrictive capacity of current battery technologies which limit flight times [20] and the potential for security attacks against the UAVs [21], [22]. While the new work in this manuscript does not specifically address these issues directly, the problems of limited battery capacity of the drone was noted during testing (three heavy-duty battery power packs were consumed during the testing) and the matter of drone security must be noted as a genuine threat against service delivery. The drone communication system for testing utilized an encrypted 9 channel point-to-point communications system despite the risk of nefarious intervention being negligible. Indeed, encrypted UAV control [23] as well as use of novel inflight charging methods [24] offer encouraging developments to mitigate against such fundamental obstacles to implementation.

This work thus presents empirical results and mathematical modeling for channel gain, mean delay (τ_{mean}), and RMS delay spread (τ_{RMS}) to characterize the radio channel between ultra-low altitude aerial vehicles and a smart communications device user for 5G cellular mobile services using mid-band frequencies (the EU license band of 3.4-3.8 GHz was used). The experiments were conducted across a range of carefully selected environments and user modes for three different ultra-low altitude drone heights. Additionally, the variance between the globally allocated 5G mid-band frequencies and bandwidths is investigated. The three selected ultra-low altitude drone heights were 5 m, 10 m, and 15 m above the ground and were specifically chosen to explore communication links for scenarios where there may be numerous miniature 5G aerial base-stations hovering just overhead or personalized close-proximity orbs supporting high-speed connectivity. Additionally, envisaged were disaster recovery zones where an ultra-low altitude communications drone would be allotted to a group of workers or a single worker - perhaps utilizing AR/VR-enabled thermal imaging and radar technologies to aid human recovery and requiring a dedicated communications link. While much 5G focus has gravitated towards the 60 GHz band, 5G cellular services will be delivered across a number of bands and the mid-band presented here is essential to understand.

This work presents an empirical study of drone-to-user communication channels for ultra-low altitudes across a range of environments. It helps to validate the potential for such temporal service arrangements as well as to help inform those deploying such 5G services by offering statistical modeling of the various channels.

II. EXPERIMENTAL ARRANGEMENTS
A. MEASUREMENT SYSTEM

For the experimental arrangement the transmitter was affixed to the underside of the drone (Fig. 1) and the receiver determined as a handheld smartphone device. The transmitter radio unit was a battery-powered Time-Domain PulsON210 source (https://timedomain.com) with a vertically-polarized electrically small UWB bottom-fed planar elliptical dipole [25]. The antenna return loss was typically –15 dB, boresight gain of 2 dBi for an isolated antenna, and a voltage standing wave ratio (VSWR) value of 1.5:1.

FIGURE 1. Commercial drone used for 5G testing.

The receiver was a corresponding PulsON210 radio unit with the same design of antenna as utilized at the transmitter. Both antennas incorporate a Balun transformer for matching and to minimize spurious cable currents [26]. Fig. 2(a) depicts the transmit antenna wideband azimuthal radiation patterns for an isolated antenna and for the antenna attached to the drone. Fig. 2(b) also presents the receive antenna for an isolated case and for the antenna incorporated into a smartphone for both popular user modes (the texting/landscape video position and the phone call position).

The propagation channel was sampled at 100 Hz with the recorded channel impulse response (CIR) data being captured on a laptop (3500 points per CIR, scan step size of 32e-12 s). This sampling rate suitably meets the Nyquist criterion for a node (drone) moving at 0.5 m · s^{-1} (the Doppler frequency is less than 10 Hz for this arrangement). Each scan was post-processed in the frequency domain by de-convolving the received CIR from a reference measurement made at a fixed transmitter–receiver separation of 3.2 m in the anechoic chamber [26]. This technique effectively removes the effects of the pulse distortion caused by the transmit-receive chains and antennas to leave only the transfer function of the radio propagation channel [26].
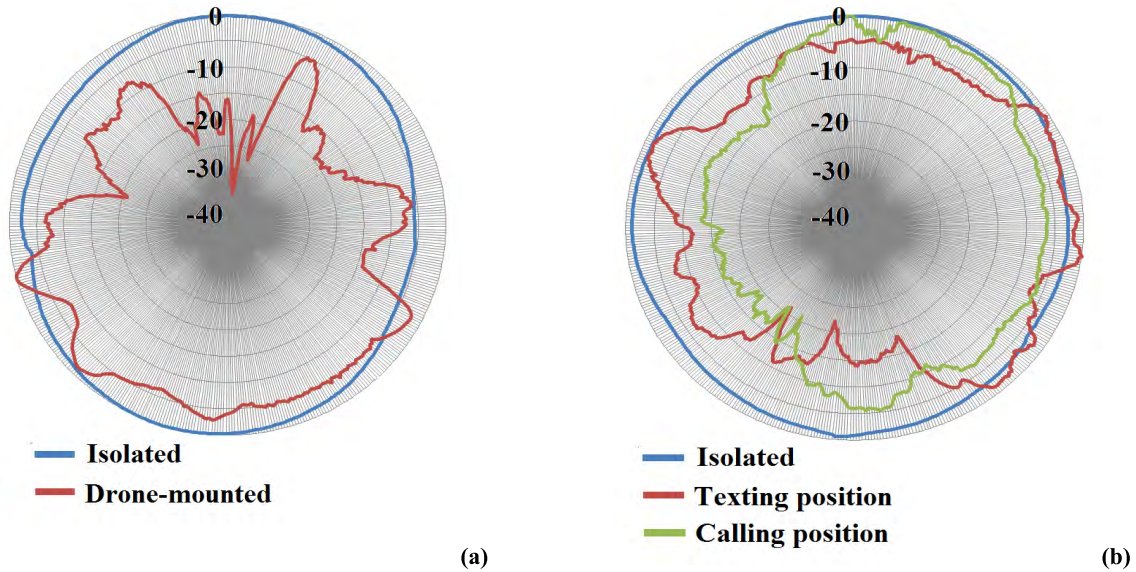
(a)

(b)

FIGURE 2. Wideband azimuthal radiation patterns. (a) Transmit antenna for an isolated case and for the antenna attached to the drone, and (b) Receive antenna for an isolated case and for the antenna incorporated into a smartphone for both popular user modes.
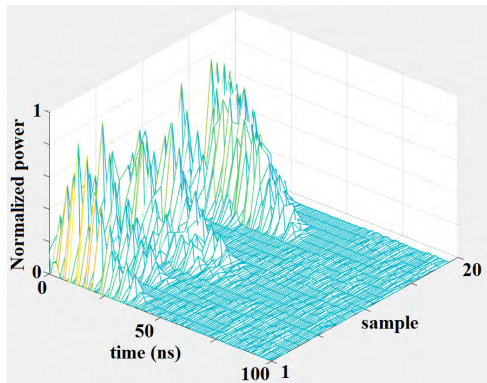

FIGURE 3. Example of Power Delay Profile (PDP) measurements presented for the drone operating in the enclosed environment (first 20 samples shown).

Each CIR was further post-processed to extract individual Power Delay Profiles (PDP) for the measurements (100 per second). The discrete components of each PDP were subject to a minimum threshold which was determined by making a series of background noise measurements; this process was to remove background noise and distortion effects. PDPs were then further processed to attain the Received Wideband Power (RWP) [27], mean delay (τ_{mean}), and Root Mean Square delay spread (τ_{RMS}); details of the computations are described in section "III. Results". The measurements were made in the time domain which has advantages over frequency domain measurements for measurements involving mobile radio terminals [28]. Table I summarizes the measurement parameters used during experimentation. Fig. 3 depicts successive PDPs being captured (5 seconds of example data in the enclosed environment shown).

TABLE 1. Test measurment parameters.

Primary 5G band	3.4-3.8 GHz (EU band)
Additional test bands	Detailed in Table V
Radio units	PulsON 210
Transmit antenna return loss	- 15 dB
Transmit antenna boresite gain	2 dBi
Transmit antenna VSWR	1.5:1
Receive antenna return loss	- 15 dB
Receive antenna boresite gain	2 dBi
Receive antenna VSWR	1.5:1
Sample rate	100 Hz
Data points per CIR	3500
Scan step size	32e-12 s
Drone velocity	0.5 ms^{-1}

B. TEST ENVIRONMENT AND ARRANGEMENTS

The frequency being considered is the recently specified mid 5G band for the European Union (3.4-3.8 GHz) [29] with a comparison being conducted across many of the global bands for a subset of the overall results. A selection of three heights were chosen; 5 m, 10 m, and 15 m above the ground where

the user is located. The drone traveled along a horizontal path starting at 10 m from the user's position and moving at a controlled speed of 0.5 ms^{-1}, stopping at 10 m on the other side of the user (as depicted in Fig. 4). The three heights provide insight on how the height of the drone may affect the propagation path and signal multipath (with Euclidean distance aspect removed as per [30] and [31]), as well as the effects of the drone at various horizontal distances from the user. Indeed, the focus of this work is specifically on ultra-low altitudes. The specific focus of the presented work was to consider scenarios of personalized base station services, communications support for rescue workers, or targeted localized temporal enhanced services. Future work may address high altitude links at 5G mid-band frequencies although such arrangements have been previously considered for 5 GHz [12] and 2.4 GHz/850 MHz [14].
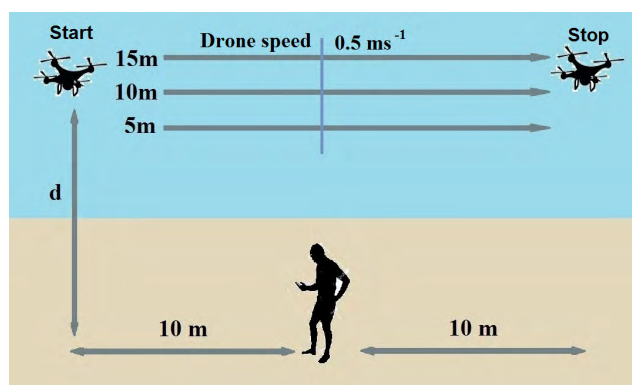

FIGURE 4. Geometrical test arrangement for the 5G drone relative to the service user (testing position shown).

Three different test environments were selected to investigate the effects of various multipath environmental factors across indicative operating scenarios. The characteristically contrasting set of environments included; an open site (field), an enclosed area bound by three sides, and a partially tree-lined area (Fig. 5) with 25 m high trees. Two distinct user modes were chosen to cover typical user operation; namely a user in the texting position (moreover used for web browsing, app use and video streaming) and also in the phone call position (device held against the right ear); this will allow two different proximities with the human body to be analyzed. For all experiments the test user was an adult male of mass 80 kg, height 1.70 m. The antenna on the drone was aligned with the direction of travel as shown in Fig. 6(a) to avoid the significant variations of the elevation plane (vertical) and instead use the more uniform azimuthal plane [25]. To complement this, the antenna orientations for both the texting and calling positions were arranged for similar predictability. These arrangements are depicted in Fig. 6(b-c) (texting orientation with respect to the drone depicted in Fig. 4) and use of these orientations help to focus the analysis on the propagation environments as opposed to a study on the specific characteristics of the antenna.

The drone used for measurements was a multi-rotor Tarrot 680 (Fig. 1) with a wing/rotor span of 800mm, 350mm diameter Z-blade propellers attached to DJI 3510 E800 motors, DJI E Series 620S electronic speed controllers, and a DJI A2 flight control system. The craft weighed 6500 grams and operated on an encrypted 9 channel 2.4 GHz command and control frequency (Spektrum DSM2 Twin receiver) and had a number of intelligent programmable flight modes to aid stability and fixed path trajectories. Throughout testing it was flown by a commercial drone pilot (from 360 Capture, N. Ireland).

The radio propagation channels for each scenario were mathematically modeled using statistical distributions of channel gain, the mean signal delay from drone to the user's devices (τ_{mean}) and the Root Mean Square delay spread of those signals (τ_{RMS}). These statistics are mathematically derived from the time-domain sequential PDPs using the first detectable received signal at the user's handset. The maximum likelihood (ML) estimates of the received 5G signal amplitudes were calculated for commonly used statistical distributions; the Akaike Information Criterion (AIC) [28] was then employed to identify the best fit statistical distribution.

Additionally, the effects of attaching a base station to a drone were investigated. Notably, the utilization of a commercial drone may affect the results compared to tests that may be conducted using other types of aerial platforms including: helium balloons, base stations suspended between buildings, and other rigs designed to mimic an operational ultra-low altitude UAV.

III. RESULTS

A. EFFECTS OF ATTACHING THE BASE STATION TO THE DRONE

The effects on the 5G base station operation (in terms of RWP, τ_{mean} and τ_{RMS}) when attached to the drone was investigated. The 5G signals from the radio unit when the drone was not operational (all electronics and communications powered down and rotors stationary) versus the operational drone (all control and wireless systems live and all six rotors turning) were compared at a fixed transmitter-receiver distance of 2 m in an open area.

Results indicate that the vibration and wireless signals from the drone have little impact on the various channel-describing parameters with the mean RWP values for the two modes almost identical; the same is also true of the respective mean τ_{mean} and τ_{RMS} values (Table II). The RWP range is slightly larger for the drone in operation as are the delay parameter ranges; this is likely due to the physical movement (vibration) of the craft however such differences are small (Table II). The standard deviation (s.d.) of all three parameters is also very similar highlighting that the effects of the drone's vibrational movement due to the rotors spinning as well as the electrical and RF noise from the operational drone has an insignificant impact on the 5G measurements being made (Table II). These statistics are reflected in Fig. 7
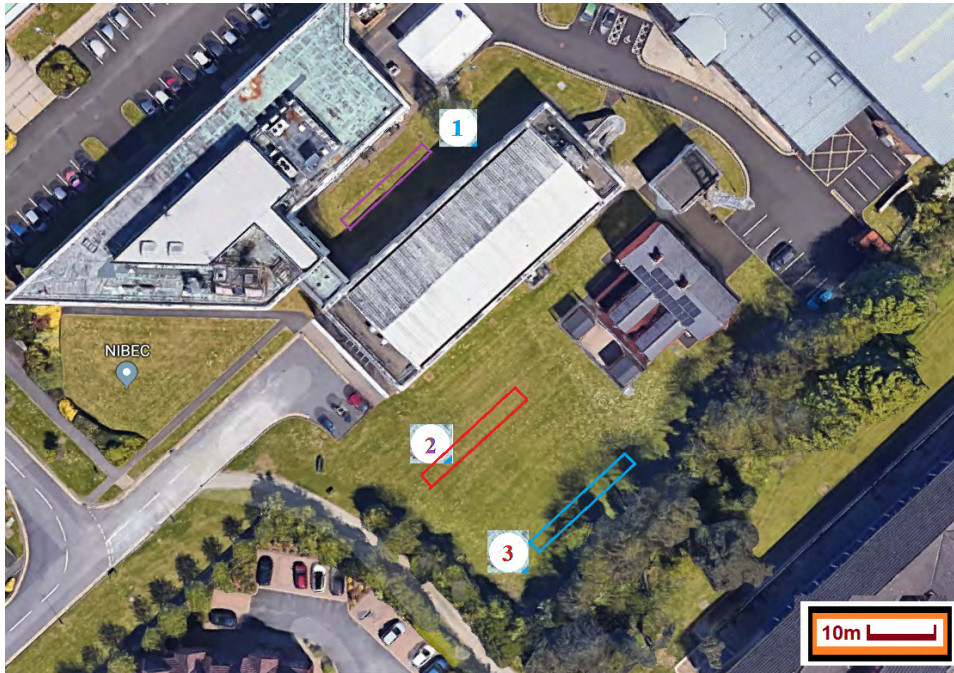
FIGURE 5. Three selected test environments - an enclosed area bound by three sides (1); an open site (2); and a partially tree-lined area (3).
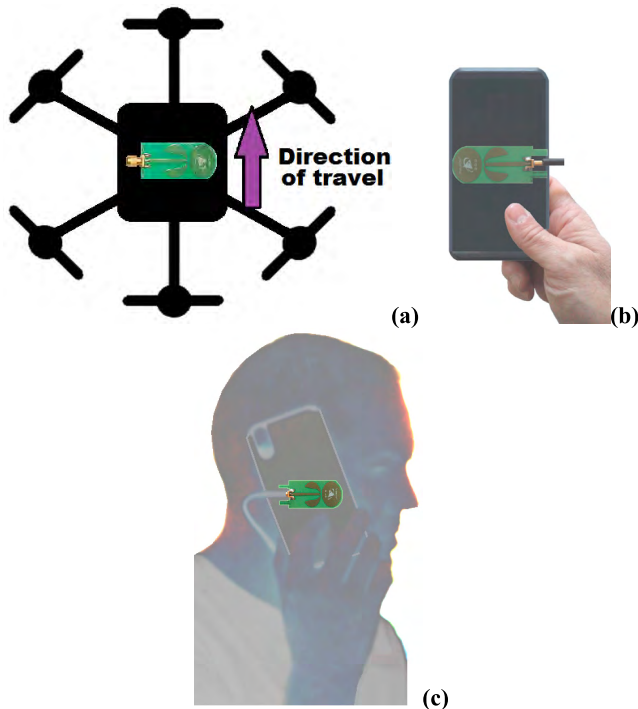

FIGURE 6. Orientations of the antennas during tests. (a) Antenna affixed to the drone with respect to the direction of travel, (b) location and orientation of the antenna for texting user mode, and (c) silhouette depicting orientation of the antenna with respect to the user and phone.
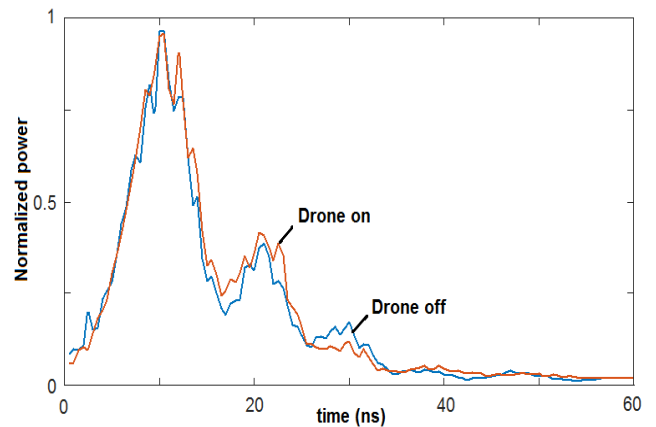

FIGURE 7. Averaged Power Delay Profile (PDP) comparison for drone in operation (with electronic circuits on and rotors at full power) versus the drone switched off (time truncated to 60 ns to enhance detail).

B. RECEIVED WIDEBAND POWER MEASUREMENTS

To process the captured raw RWP data, the various combinations and permutations of height/user mode/location were analyzed for receive signal strength measurements from the aerial base station to the user's device. A moving average window was implemented to remove the inherent path loss effects (de-mean the signal) as recommended by Clarke [31]. The received power encapsulates both fast and slow fading; demeaning thus serves to eliminate the local mean which removes the contribution from slow fading variations. A window size of 7.5 λ was used (100 data points) as recommended in [32].

(time truncated to 60 ns for clarity) which depicts the averaged PDPs for the drone in full operation versus the drone switched off.

TABLE 2. Comparative results for received wideband power, τ_{mean}, and τ_{RMS} values for the drone in operation versus drone switched off.

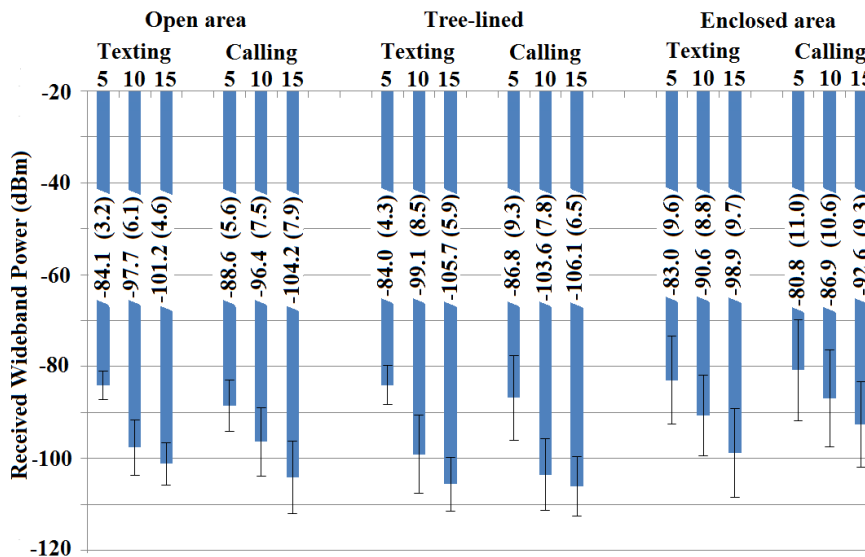|	Mean			Range			s.d.		
	RWP	τ_{mean}	τ_{RMS}	*RWP*	τ_{mean}	τ_{RMS}	*RWP*	τ_{mean}	τ_{RMS}
OFF	-101.4	13.2 ns	15.5 ns	5.8	0.97 ns	2.21 ns	1.2	0.22 ns	0.54 ns
ON	-101.2	13.3 ns	15.4 ns	8.2	1.15 ns	3.13 ns	1.5	0.23 ns	0.64 ns

FIGURE 8. Average received wideband power (dBm) and standard deviation value (in brackets) for each arrangement.

The PDP of each sample is obtained as the spatial average of the complex baseband CIR of each sample [33] and defined as

$$P(\tau) = \sum [|h(t, \tau)|^2] \qquad (1)$$

where h is the channel impulse response. The total received wideband power of a PDP can be determined by the sum of the squares of all the amplitudes (all the power) in the PDP [34], [35], as presented in (2).

$$P_{[dB]} = 20 log_{10} \left(\sum_{j=1}^{N} \langle a_j \rangle \right) \qquad (2)$$

where N is the nth incident pulse and a is the amplitude of the nth incident pulse.

For each experimental scenario the maximum likelihood (ML) estimates of each parameter were calculated for popular statistical distributions and the Akaike Information Criterion (AIC) utilized to determine the closest fitting distribution [36]. Fig. 8 presents the mean RWP values as well as the s.d. of the spread of RWP values for each particular test arrangement. The datasets were transformed into a Cumulative Distribution Function (CDF) with bins assigned according to the Freedman-Diaconis rule (Fig. 9). Table III displays the best fit mathematical distribution and the associated descriptive parameters for that distribution. For all of the

environmental scenarios, user test modes, and drone heights the distribution of the RWP values was best modeled by the Rician distribution. Rician probability distribution function ($P(r)$) is typically best used where a dominant specular component exists [37]; such geometry exists across many of the tests due to the aerial nature of the transmitting radio set. This indicates that for such arrangements in the mid-5G band the drone-user links are comparable to direct line-of-sight links. The Rician distribution is mathematically expressed below in (3), (4);

$$P_{(r)} = \frac{r}{\sigma^2} \cdot e^{\left(\frac{r^2 + r_s^2}{\sigma^2}\right)} \cdot \boldsymbol{B} \qquad (3)$$

where;

$$\boldsymbol{B} = I_o(r \cdot r_s / \sigma^2) \qquad (4)$$

where B is the modified Bessel function, σ^2 is the mean power of multipath components, r is the data series being modeled, and r_s is the dominant component power (dominant wave) [38]. The parameter estimates (s, σ) and their standard error are expressed in Table III for each experimental arrangement.

Results in Fig. 8 depicted how the RWP values decreased with increasing height which is expected as the RWP is a function of the transmitter-receiver separation -- this is a standard result based on the basic principles of signal propagation and is entirely expected.
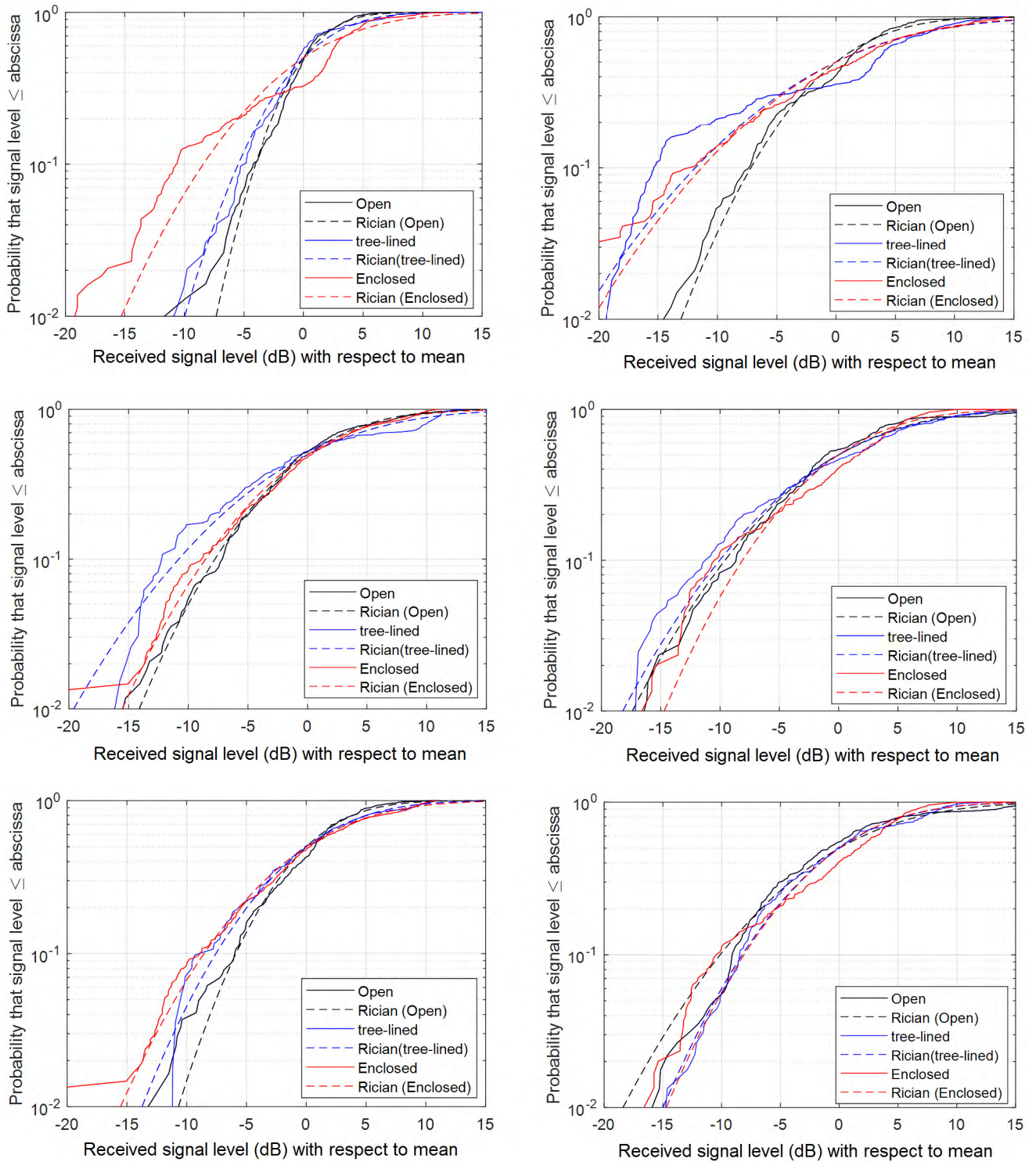
FIGURE 9. Cumulative Distribution Function of received wideband power (and best fit mathematical distribution for various user modes and drone heights. Top left Texting with drone at 5m, Top right Texting with drone at 10m, Centre left Texting with drone at 15m, Centre right Calling with drone at 5m, Bottom left Calling with drone at 10m, Bottom right Calling with drone at 15m.

Observing the two user modes across all tests it was ascertained that the texting position had higher RWP values than the phone call position for the open environment and the tree-lined environment, although the reverse was true for the

enclosed area. For the texting position the receive antenna is less affected by body shadowing effects and antenna detuning due to close proximity with the human body. In the enclosed area the increased reflecting and scattering environmental

TABLE 3. Summary of results for received wideband power presenting the best fitting statistical distribution, and the corresponding model's descriptive shape parameters.

Environment	User mode	Height	Distribution	Statistical parameters			
				Est.	Std. Err.	Est.	Std. Err.
Open area	Text	5	Rician	s= -84.1	s= 0.187	σ= 3.195	σ= 0.132
		10	Rician	s= -97.7	s= 0.330	σ= 6.071	σ= 0.234
		15	Rician	s= -101.2	s= 0.295	σ= 4.600	σ= 0.209
	Call	5	Rician	s= -88.6	s= 0.308	σ= 5.623	σ= 0.218
		10	Rician	s= -96.4	s= 0.469	σ= 7.489	σ= 0.332
		15	Rician	s= -104.2	s= 0.528	σ= 7.923	σ= 0.373
Near trees	Text	5	Rician	s= -84.0	s= 0.307	σ= 4.292	σ= 0.217
		10	Rician	s= -99.1	s= 0.607	σ= 8.444	σ= 0.429
		15	Rician	s= -105.7	s= 0.560	σ= 5.914	σ= 0.396
	Call	5	Rician	s= -86.8	s= 0.559	σ= 9.275	σ= 0.395
		10	Rician	s= -103.6	s= 0.549	σ= 7.841	σ= 0.389
		15	Rician	s= -106.1	s= 0.431	σ= 6.454	σ= 0.305
Enclosed arena	Text	5	Rician	s= -83.0	s= 0.315	σ= 6.577	σ= 0.223
		10	Rician	s= -90.6	s= 0.226	σ= 4.775	σ= 0.160
		15	Rician	s= -98.9	s= 0.287	σ= 6.686	σ= 0.203
	Call	5	Rician	s= -80.8	s= 0.327	σ= 5.834	σ= 0.232
		10	Rician	s= -86.9	s= 0.371	σ= 6.572	σ= 0.262
		15	Rician	s= -92.6	s= 0.367	σ= 6.332	σ= 0.260

characteristics increases the complexity of the body's effect on the signal path and thus the same correlation is not observed.

Indeed, when the three 5G environments are considered for mean RWP values the enclosed area presents the highest RWP levels, followed by the tree-lined and then the open environments respectively (Fig. 8). This strongly correlates with the multipath characteristics of each environment.

The s.d. of the RWP values were scrutinized to obtain an understanding of the spread of values in each operating environment (Fig. 8). It was discovered that no correlation between drone height and s.d. of the RWP values existed. The s.d. values of the texting arrangement were less than those of the call arrangement across all environments and heights as holding the radio system to the head typically increases antenna detuning effects (this antenna was not optimized for wearable operation) as well as an amount of body shadowing, as understood from Fig. 2(b).

The s.d. of the RWP values was greatest in the enclosed area due to the changing multipath interference effects as the drone traversed the set route. The s.d. was less in the tree-lined test area and less again in the open area. In the tree-lined area there will be some reflection off the trees as well as an amount of refraction; this is supported by the mean delay results. These outcomes infer that high multipath environments such as enclosed areas, urban settings, etc. will generally enjoy higher RWP receive levels but also suffer from significant fades compared to lower multipath environments.

As these tests involve a moving terminal the overall RWP values will be a composite of large-scale path loss fading effects due to the terminal distance separation effects and the small-scale path loss effects which are a result of the characteristics of the specific environment and subtitle movements of the drone unit. To further explore the small-scale path loss effects which better describe the environment-specific fluctuation of signal losses due it is required that the large-scale fading distance separation effects are removed using the Friis equations with a path loss exponent of 2 as per [12] and [39] (processed in Matlab and considering the transmitter-receiver separation across the full drone journey paths). When this small scale analysis technique is applied it is discovered the small-scale signal fading mean RWP and the different drone heights can be generally observed to reduce in power for increasing drone height; this is after the distance effects have been removed already (a graph of outcome not presented for brevity, however the path loss attributed to transmitter-receiver separations of 5m, 10 m, and 15 m are -57.6 dB, −63.6 dB, and −67.1 dB respectively). This indicates there are deeper fades at the higher altitudes due to multipath effects created by the changing geometry. It is noted that the difference in RWP between 5 m and 10 m is clear, but between 10 m and 15 m is less well correlated. This further suggests that as the height increases the small-scale effects reduce.

Fig. 9 CDF shows the distribution of the RWP values for each test and the respective best fit models. These are normalized at 0 dB for comparison using the mean value of the dataset as per [31] and [32]. Fig. 8 indicates that a range of 35 dB from the strongest to the weakest received signal strength is typical across the tests. With respect to the three heights investigated, it is observed in Fig. 9 that as the height increased the quality of model fit gets slightly better; this can be attributed to a less strong ground bounce effect as well as fewer fluctuations in signal as height increases. This

furthermore supports the conclusion that small-scale effects reduce as the height increases.

For the two user modes the model fits are better for the calling user mode than the texting mode (Fig. 9). The spread of values was similar across both modes although the CDFs for the calling mode generally show a smaller difference between the environments than for the texting position (open vs enclosed values). This is likely due to the body signal absorption reducing the multipath propagation for the environments with the higher inherent multipath (enclosed will have the most reflections and the open area the least).

C. CHANNEL DELAY PARAMETERS

The channel delay parameters are devised into two categories. Temporal spreads (time dispersion) of the radio channel are derived from power delay profiles [40]. The mean excess delay is the first central moment of the power-delay profile (PDP) and describes the average propagation delay relative to the first-arriving signal component [37].

$$\tau_{mean} = \frac{\sum\limits_{i=0}^{\infty} \tau_i P(\tau_i)}{\sum\limits_{i=0}^{\infty} P(\tau_i)} \qquad (5)$$

where τ_{mean} is the mean excess delay (average delay), τ_i is the time delay of the ith path and $P(\tau_i)$ is the channel impulse response.

The RMS delay spread (τ_{RMS}) is a measure of the temporal spread of the PDP about the mean excess delay. These parameters are the most commonly used to describe wideband multipath channels [41].

$$\tau_{RMS} = \sqrt{\frac{\sum\limits_{i=0}^{\infty} (\tau_i - \tau_m)^2 P(\tau_i)}{\sum\limits_{i=0}^{\infty} P(\tau_i)}} \qquad (6)$$

Fig. 10 and Fig. 12 present the averaged (mean) τ_{mean} and τ_{RMS} values respectively as well as the s.d. of those values. As before, the results were transformed into a CDF using bins assigned according to the Freedman-Diaconis rule [36] and ML estimates of each parameter were calculated for popular statistical distributions and the AIC employed for selection. CDFs for τ_{mean} and τ_{RMS} are displayed in Fig. 11 and Fig. 13 respectively and visualize the average τ_{mean} values and the characteristics of the spread of results.

Table IV displays the best fit mathematical distribution and the associated descriptive parameters for that distribution. The open and tree-lined areas were each best described by the Weibull statistical distribution for both τ_{mean} and τ_{RMS} parameters across both types of user modes. The Weibull statistical distribution is of the form

$$P_{(\tau)} = \frac{\alpha}{\beta} \left(\frac{r}{\beta}\right)^{\alpha-1} \cdot e^{\left(\frac{r}{\beta}\right)^{\alpha}} \qquad (7)$$
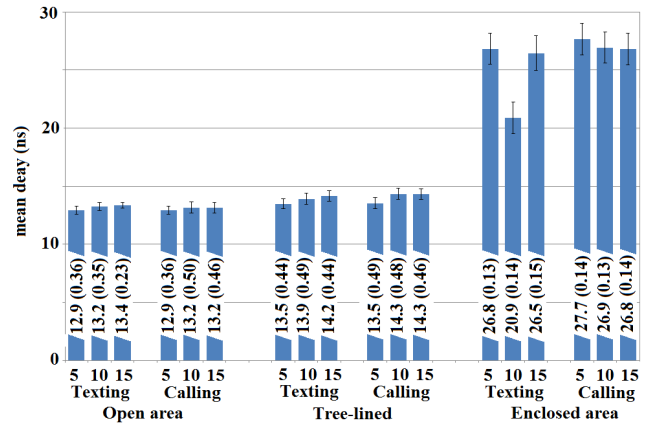
FIGURE 10. Average Mean delay (ns) and standard deviation value (in brackets) for each arrangement.

where r is the data series being modeled, α is the model shape parameter, and β is the model scale parameter, with α and β relating to model descriptors β *and* α in Table IV.

Weibull can be useful when the transmitter or receiver are mobile in the environment [42], as the Weibull fading parameter β increases, the severity of the fading increases [43]. The β is the scale parameter and directly linked with the frequency of values at each sample bin and thus the average values for both τ_{mean} and τ_{RMS} values across both the open area and tree-lined area (Fig. 11 and Fig. 13).

As the drone height increases the values of β increase for τ_{mean} and decrease for τ_{RMS} (Table IV). This correlates strongly with the increasing height causing more multipath components due to the changing geometry as well as a reduced delay spread due to the reducing signal power. As the mean delay is referenced against the first arriving signal [37], the increasing vertical distance between the transmitter and receiver units creates a change in geometry and thus increases the radial signal area around the ground-based receiver as discussed by Al-Hourani *et al.* [44]. This effectively incorporates a greater area for multipath components to add to the overall received signal.

The s.d. values (Fig. 10) indicate that the tree-lined site has slightly higher s.d. values compared to the open area. As the Weibull scaling factor (β) increases, the spread of the values also increases and thus the s.d. will also increase resulting in higher τ_{mean} average values. This phenomenon correlates directly with the increase in reflecting and scattering surfaces in the tree-lines environment compared to the open area. Weibull shape (α) values of the τ_{mean} values (Table IV) were generally higher for the tree-lined environment compared to the open area (for the call user mode particularly). This is due to the increased signal reflection off the nearby trees.

The Weibull shape α values for the τ_{RMS} figures are generally higher for the tree-lined environment compared to the open area (Table IV). This pattern of results is due to the increased number of signal reflectors in the tree-lined site. With respect to the varying heights of the 5G drone no significant correlation exists in the τ_{RMS} average values.
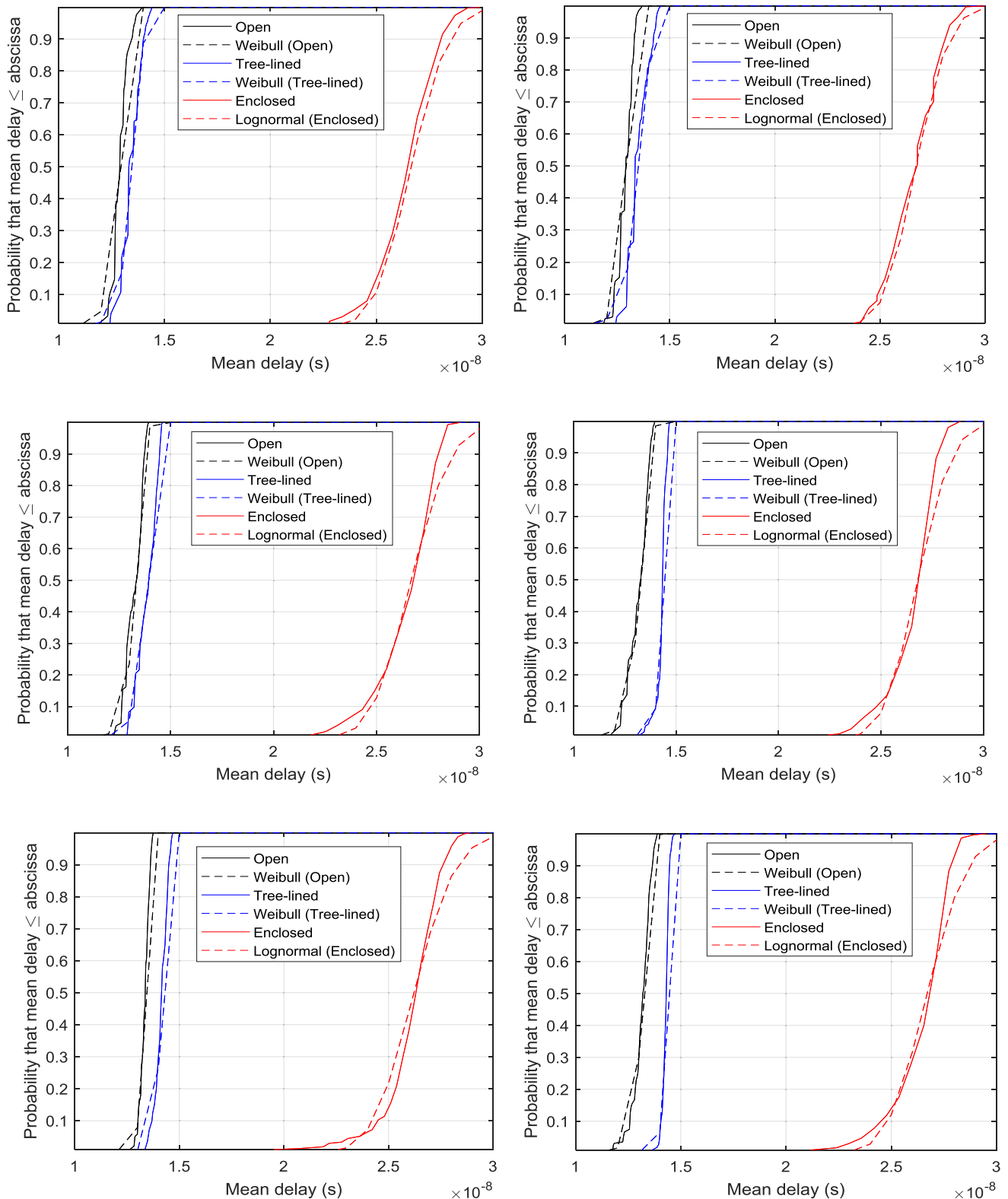
FIGURE 11. Cumulative Distribution Function of $\tau_{\mathbf{mean}}$ and best fit mathematical distribution for various user modes and drone heights. Top left Texting with drone at 5m, Top right Texting with drone at 10m, Centre left Texting with drone at 15m, Centre right Calling with drone at 5m, Bottom left Calling with drone at 10m, Bottom right Calling with drone at 15m.

Likewise, there was no notable difference between the τ_{RMS} average values for the texting and call positions for all test arrangements. The τ_{RMS} Weibull shape α values for the various heights illustrate a small correlation for decreasing α values and increasing height for the tree-lined scenario and no notable correlation in the open area. This indicates that the
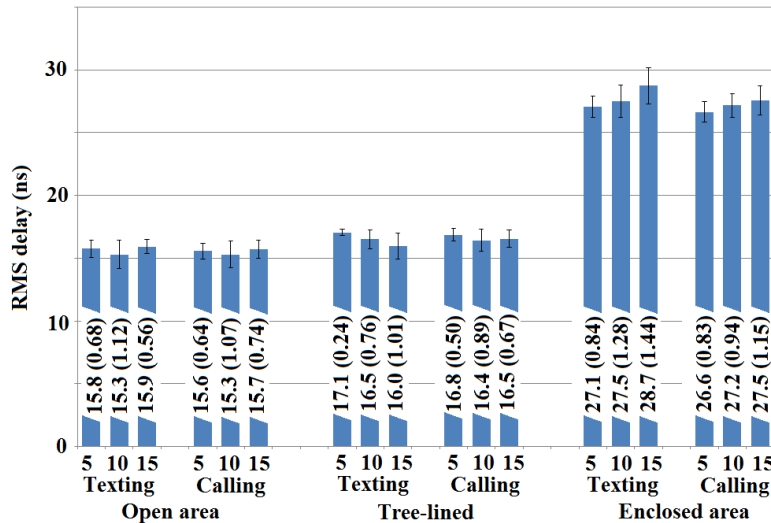
FIGURE 12. Average Root Mean Square delay spread (ns) and standard deviation value (in brackets) for each arrangement.

trees have an effect on the α values as height changes. Increasing drone height increases the path length of the reflected signal from the trees with respect to the direct signal path (i.e. changing geometry).

The enclosed arena environment was best described by the Lognormal mathematical distribution for both user modes for τ_{mean} and also τ_{RMS}. The statistical parameters of each fit are presented in Table IV and describe the shape and characteristics of the best fitted distribution. Lognormal is often used when long-term variations are caused by gross variations in the physical environment between the transmitter and receiver, or when the transmitter or receiver moves to a different location [45]. Generally, the nature of the enclosed arena ensures multiple reflected versions of the original signal which increases the signal delay periods and increases the chance for message interference at the receiver. Lognormal distributions are defined by having a predominant number of lower value components; in this specific case a relatively larger number of shorter mean delays and RMS delay spread values compared to the overall spread of values. This is because most of the significant signal arrives in the main direct path and in the initial subsequent reflections. As the enclosed area has good signal reverberation characteristics there are further weaker reflected versions of the signal arriving some time later. This increases the mean delays and RMS delay spread values as both channel indicators are derived with respect to the channel impulse response (which contains signal amplitude information) of the signal which significantly diminishes as the signal reverberates in the enclosed environment. The Lognormal statistical distribution is expressed as

$$P_{(r)} = \frac{1}{r \cdot \sigma \sqrt{2\pi}} \cdot e^{\left\{ \frac{-(\ln r - \mu)^2}{2\sigma^2} \right\}} \qquad (8)$$

where r is the data series being modeled, σ is the standard deviation of r, and μ is the mean of the values of r expressed

in dB. The parameter estimates (μ, σ) and their standard error are expressed in Table IV for each experimental arrangement.

For the two user modes across all environments the call position has a slightly greater average τ_{mean} value than the texting posture (Fig. 10). This may be due to the differing ground bounce distances of the first reflected ray. The enclosed area displays a larger average τ_{mean} than the tree-lined area with the open area presenting the lowest average τ_{mean} values. This is a direct effect of the geometry of the environmental reflectors.

From Fig. 11, it is observable that the best fit models have some deviation between the model and empirical results at the higher end of the mean delay values (particularly for the results from the enclosed area). The CDFs highlight a distinction between the enclosed environment and both the open and tree-lined environments. The delay is greater for the enclosed area due to the increased signal reverberation effect of the electrically reflective environment which offers a greater number of nearby signal reflectors compared to the other environments. This results in the higher τ_{mean} values (Fig. 10). The enclosed environment also had the greatest spread of values (Fig. 10) due to multiple reflected signals arriving some time after the initial primary signal was received.

With regards to the two user modes, the CDFs show little difference in τ_{mean}. Fig. 10 indicates a higher s.d. of values between the two modes for the open area (with the calling position having higher s.d. values), but with very similar s.d. values in the other environments. This would denote that environments with greater multipath reflectors are less affected by varying user postures. This relationship can be ascertained from Fig. 10 but is more obvious from the numerical values of Fig. 11. These results allow us to better understand how the 5G radio channel between the drone and the user is affected for the various user modes and environments. Extended delays can cause issues for the cellular system as heavily delayed versions of previous signal components can

TABLE 4. Summary of results for τ_{mean}, and τ_{RMS} presenting mean values, standard deviation, the best fitting statistical distribution, and the corresponding model's shape parameters.

Environment	User mode	Height	delay parameter	Distribution	Statistical parameters			
					Est.	Std. Err.	Est.	Std. Err.
Open area	Text	5	τ_{mean}	Weibull	β= 1.29E-08	β= 5.81E-12	α=34.283	α=1.381
			τ_{RMS}	Weibull	β= 1.58E-08	β= 7.46E-12	α=32.236	α=1.545
		10	τ_{mean}	Weibull	β= 1.32E-08	β= 5.09E-12	α=37.830	α=1.668
			τ_{RMS}	Weibull	β= 1.53E-08	β= 1.25E-11	α=18.046	α=0.830
		15	τ_{mean}	Weibull	β= 1.34E-08	β= 3.23E-12	α=70.566	α=3.541
			τ_{RMS}	Weibull	β= 1.59E-08	β= 6.96E-12	α=39.099	α=2.112
	Call	5	τ_{mean}	Weibull	β= 1.29E-08	β= 4.46E-12	α=42.287	α=1.785
			τ_{RMS}	Weibull	β= 1.56E-08	β= 7.64E-12	α=29.859	α=1.307
		10	τ_{mean}	Weibull	β= 1.32E-08	β= 6.61E-12	α=33.380	α=1.690
			τ_{RMS}	Weibull	β= 1.53E-08	β= 1.36E-11	α=18.944	α=0.991
		15	τ_{mean}	Weibull	β= 1.32E-08	β= 6.06E-12	α=38.398	α=2.017
			τ_{RMS}	Weibull	β= 1.57E-08	β= 9.67E-12	α=28.882	α=1.596
Near trees	Text	5	τ_{mean}	Weibull	β= 1.35E-08	β= 7.43E-12	α=33.182	α=1.776
			τ_{RMS}	Weibull	β= 1.71E-08	β= 3.04E-12	α=100.874	α=5.840
		10	τ_{mean}	Weibull	β= 1.39E-08	β= 7.27E-12	α=34.927	α=2.025
			τ_{RMS}	Weibull	β= 1.65E-08	β= 1.01E-11	α=29.879	α=1.808
		15	τ_{mean}	Weibull	β= 1.42E-08	β= 6.14E-12	α=55.300	α=4.095
			τ_{RMS}	Weibull	β= 1.60E-08	β= 1.91E-11	α=20.330	α=1.577
	Call	5	τ_{mean}	Weibull	β= 1.35E-08	β= 7.28E-12	α=28.663	α=1.281
			τ_{RMS}	Weibull	β= 1.68E-08	β= 4.51E-12	α=56.212	α=2.885
		10	τ_{mean}	Weibull	β= 1.43E-08	β= 3.21E-12	α=78.336	α=4.303
			τ_{RMS}	Weibull	β= 1.64E-08	β= 1.08E-11	α=26.945	α=1.616
		15	τ_{mean}	Weibull	β= 1.43E-08	β= 2.41E-12	α=100.231	α=4.943
			τ_{RMS}	Weibull	β= 1.65E-08	β= 7.94E-12	α=35.185	α=1.961
Enclosed Arena	Text	5	τ_{mean}	Lognormal	μ= -19.480	μ= 3.16E-04	σ=6.59E-03	σ= 2.24E-04
			τ_{RMS}	Lognormal	μ= -19.468	μ= 1.90E-03	σ=3.96E-02	σ= 1.34E-03
		10	τ_{mean}	Lognormal	μ= -19.479	μ= 3.41E-04	σ=7.19E-03	σ= 2.41E-04
			τ_{RMS}	Lognormal	μ= -19.451	μ= 2.80E-03	σ=5.91E-02	σ= 1.98E-03
		15	τ_{mean}	Lognormal	μ= -19.497	μ= 6.44E-04	σ=1.50E-02	σ= 4.56E-04
			τ_{RMS}	Lognormal	μ= -19.393	μ= 2.78E-03	σ=6.48E-02	σ= 1.97E-03
	Call	5	τ_{mean}	Lognormal	μ= -19.462	μ= 3.20E-04	σ=5.98E-03	σ= 2.40E-04
			τ_{RMS}	Lognormal	μ= -19.444	μ= 2.14E-03	σ=4.16E-02	σ= 1.66E-03
		10	τ_{mean}	Lognormal	μ= -19.475	μ= 3.48E-04	σ=6.18E-03	σ= 2.47E-04
			τ_{RMS}	Lognormal	μ= -19.463	μ= 2.51E-03	σ=4.45E-02	σ= 1.78E-03
		15	τ_{mean}	Lognormal	μ= -19.478	μ= 4.06E-04	σ=7.00E-03	σ= 2.87E-04
			τ_{RMS}	Lognormal	μ= -19.446	μ= 3.03E-03	σ=5.23E-02	σ= 2.15E-03

interfere with current components at the receiver causing distortion or signal losses.

The RMS delay spread (Fig. 12) for each arrangement was studied in conjunction with the CDFs for τ_{RMS} (Fig. 13) and the results show that there is no identifiable correlation between τ_{RMS} values and drone height for the open and tree-lined areas for the heights explored. There appears to be a weak correlation between τ_{RMS} values and drone height for the enclosed environment with the τ_{RMS} values generally increasing as the drone height increases. Fig. 13 highlighted better goodness of fit for the best fit models of the calling user arrangement than for texting modes as the position of

the user's body helps to remove some of the weaker signals through absorption (which are typically those scenarios with a longer signal path between the transmitter and receiver and thus create a larger delay and spread of delay.

When the environments were compared (Fig. 12) it was evident that the enclosed space had a notably larger average τ_{RMS} value compared with the tree-lined area, with the open area displaying the smallest value. The CDFs (Fig. 13) support that the enclosed area yields greater values than either the open or tree-lined areas. The open or tree-lined areas have similar results and CDF shapes due to their general similarity (that is, significant amount of
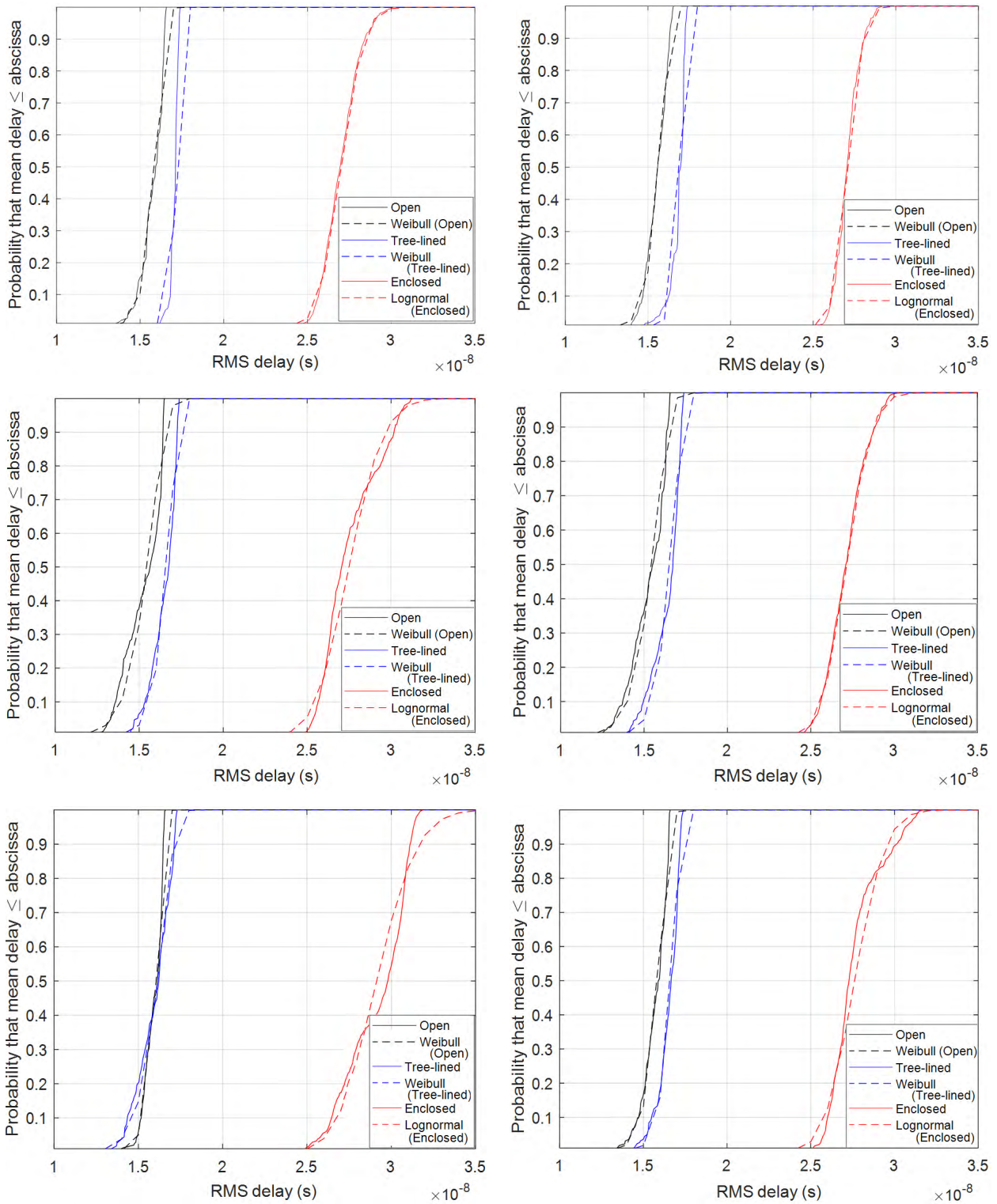
FIGURE 13. Cumulative Distribution Function of τ_{RMS} and best fit mathematical distribution for various user modes and drone heights. Top left Texting with drone at 5m, Top right Texting with drone at 10m, Centre left Texting with drone at 15m, Centre right Calling with drone at 5m, Bottom left Calling with drone at 10m, Bottom right Calling with drone at 15m.

open space in the environment). This pattern of results is correlated with the strength of the multipath environment with the enclosed area having the largest number of reflectors, scatterers, etc. These results illustrate how the different

arrangements can affect the spread of the delays; this is important to understand as it allows effective computer modeling of ultra-low altitude drone communications at these frequencies.

TABLE 5. Comparison of mean received wideband power and received wideband power standard deviation for regionally allocated bands (The Open environment was selected as an example).

| Environment | User mode | Height | delay parameter | Region | | | | | | | | | Mean deviation |
				EU 3.4-3.8 GHz	China 3.3-3.6 GHz	China 4.4-4.5 GHz	China 4.8-4.99 GHz	Japan 3.6-4.2 GHz	Japan 4.4-4.9 GHz	Korea 3.4-3.7 GHz	US 3.1-3.55 GHz	US 3.7-4.2 GHz	
Open area	Text	5	mean	-84.4	-85.0	-82.2	-86.2	-88.5	-88.6	-84.1	-82.3	-87.2	**2.28**
			std. dev.	4.21	7.18	9.71	9.67	5.26	8.26	5.07	6.87	5.73	**3.01**
		10	mean	-97.7	-100.3	-95.7	-97.5	-99.2	-100.5	-98.3	-101.2	-97.4	**1.69**
			std. dev.	6.08	6.78	8.62	9.40	7.54	7.87	6.27	6.26	7.97	**1.51**
		15	mean	-101.2	-103.0	-97.6	-95.1	-100.0	-102.1	-102.2	-110.3	-98.1	**3.35**
			std. dev.	4.61	6.61	8.76	9.35	7.55	8.27	5.58	5.90	8.30	**2.93**
	Call	5	mean	-88.6	-88.9	-88.6	-89.7	-90.1	-93.9	-88.1	-95.4	-91.7	**2.34**
			std. dev.	5.63	6.06	8.94	8.42	5.84	10.00	5.84	6.08	6.05	**1.52**
		10	mean	-96.4	-97.6	-96.9	-95.6	-98.7	-97.0	-96.3	-97.8	-97.1	**0.94**
			std. dev.	7.49	6.26	11.95	14.44	9.77	12.03	7.01	5.10	10.37	**3.15**
		15	mean	-104.2	-103.8	-104.8	-102.4	-105.5	-106.5	-104.5	-107.9	-104.0	**1.33**
			std. dev.	7.92	6.46	12.99	13.64	11.27	11.70	7.26	5.44	12.15	**3.34**
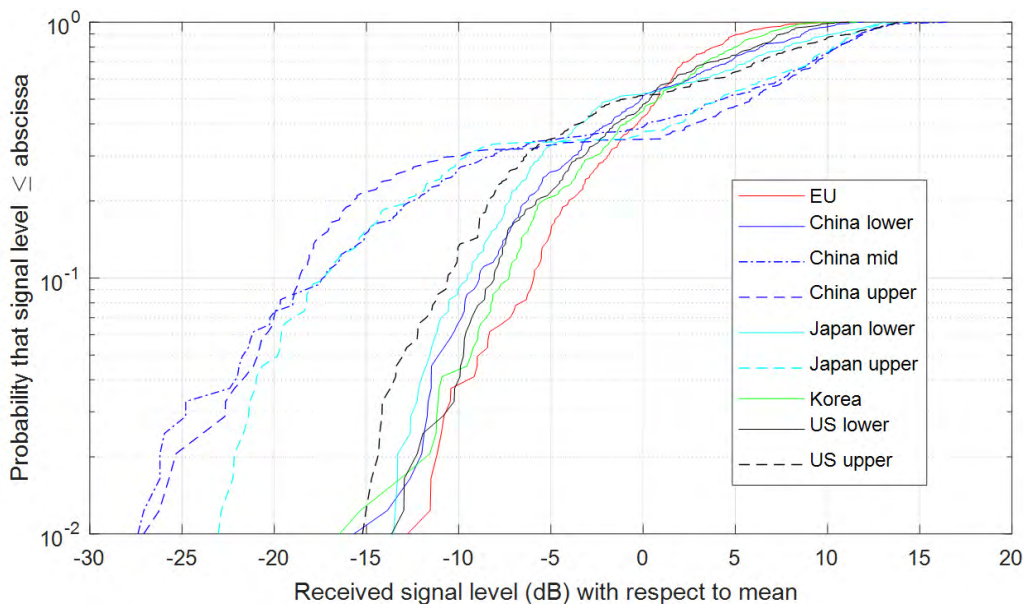
FIGURE 14. Comparison of received wideband power for regionally allocated bands (the Open environment for a texting user with a drone height of 15m compared as an example).

D. GLOBAL BAND COMPARISONS

The wideband data between 3-5 GHz was separated into the various global operating bands as depicted in Table V; globally allocated mid-5G bands for Europe, China, Japan, Korea, and North America are considered. RWP across the open environment for both a texting user mode and a phone call user mode at the three different drone heights was selected (as indicative of the band differences and for the sake of brevity). The comparison was to investigate the impact that the different center frequency and bandwidth of the various global bands may have on the presented EU band results in terms of channel gain. The comparison helps to discover how the use of a particular 5G operating frequency and bandwidth may affect the results when the same test set-up is maintained.

Based on the sampled RWP for the open environment it was observed that some variation in results was determined with the lower bands (3.1-3.8 GHz bands) having generally less s.d. and slightly less received power whereas the higher bands (3.7-4.99 GHz bands) have generally larger s.d. values and higher RWP, as presented in Table V. The unpresented results for the other user modes, drone heights and environments depict similar general characteristics. Fig. 14 also compares the distribution characteristics for a further subset of the results (15 m drone height for a texting user, again selected to be generally indicative and for brevity; other user modes, drone heights and environments depict similar patterns). The results presented in Fig. 14 indicate three allocated frequency bands that exhibit higher propagation losses than the others tested; they are the mid and upper bands for China and the upper band for Japan. It is noted that these three bands use frequencies on or above 4.4 GHz. Overall the mean deviation of RWP and s.d. results across all current bands was relatively small. The same pattern was observed for the various delay parameters with little noteworthy deviations — details

of the delay parameters are not presented for brevity. This suggests that test results for EU bands, or any of the bands, may be generally applicable to the other mid-5G bands of similar frequency and bandwidth, although it may not be judicious to rely upon such assumptions to create accurate models.

IV. CONCLUSIONS

This paper has presented the results and analysis of an empirical measurement campaign to characterize the 5G radio channel for links between an ultra-low altitude aerial base station in the form of a drone and a user's 5G device. Two user modes across three different environments with three different drone heights were considered. Maximum likelihood estimates for the various drone heights, user modes, and operational environments were found to be Rician distributed for received wideband power, whereas τ_{mean} and τ_{RMS} for the open and tree-lined environments were Weibull distributed with the enclosed area tests Lognormally distributed. Additionally, the regional variants of this mid- 5G band were found to yield minimal variance for the environments considered.

ACKNOWLEDGMENT

REFERENCES

[1] H. C. Nguyen, R. Amorim, J. Wigard, I. Z. Kovács, T. B. Sørensen, and P. E. Mogensen, "How to ensure reliable connectivity for aerial vehicles over cellular networks," *IEEE Access*, vol. 6, pp. 12304–12317, 2018.

[2] J. A. L. Calvo, G. Alirezaei, and R. Mathar, "Wireless powering of drone-based MANETs for disaster zones," in *Proc. IEEE Int. Conf. Wireless Space Extreme Environ. (WiSEE)*, Montreal, QC, Canada, Oct. 2017, pp. 98–103.

[3] M. Mezzavilla *et al.*, "Public safety communications above 6 GHz: Challenges and opportunities," *IEEE Access*, vol. 6, pp. 316–329, Feb. 2018.

[4] A. M. Hayajneh, S. A. R. Zaidi, D. C. McLernon, M. Di Renzo, and M. Ghogho, "Performance analysis of UAV enabled disaster recovery networks: A stochastic geometric framework based on cluster processes," *IEEE Access*, vol. 6, pp. 26215–26230, 2018.

[5] S. Fujii *et al.*, "Integration of drones' communication into an ITS network," in *Proc. Int. Conf. Intell. Inf. Biomed. Sci. (ICIIBMS)*, Okinawa, Japan, Nov. 2017, pp. 43–44.

[6] D. Rautu, R. Dhaou, and E. Chaput, "Maintaining a permanent connectivity between nodes of an air-to-ground communication network," in *Proc. 13th Int. Wireless Commun. Mobile Comput. Conf. (IWCMC)*, Valencia, Spain, Jun. 2017, pp. 681–686.

[7] M. Gharibi, R. Boutaba, and S. L. Waslander, "Internet of drones," *IEEE Access*, vol. 4, pp. 1148–1162, 2016.

[8] M. A. Russon. (2016). *Nokia and EE Trial Mobile Base Stations Floating on Drones to Revolutionise Rural 4G Coverage*. [Online]. Available: http://www.ibtimes.co.uk/nokia-ee-trial-mobile-base-stations-floatingdrones-revolutionise-rural-4g-coverage-1575795

[9] S. A. R. Naqvi, S. A. Hassan, H. Pervaiz, and Q. Ni, "Drone-aided communication as a key enabler for 5G and resilient public safety networks," *IEEE Commun. Mag.*, vol. 56, no. 1, pp. 36–42, Jan. 2018.

[10] R. Amorim, H. Nguyen, P. Mogensen, I. Z. Kovács, J. Wigard, and T. B. Sørensen, "Radio channel modeling for UAV communication over cellular networks," *IEEE Wireless Commun. Lett.*, vol. 6, no. 4, pp. 514–517, Aug. 2017.

[11] A. Al-Hourani and K. Gomez, "Modeling cellular-to-UAV path-loss for suburban environments," *IEEE Wireless Commun. Lett.*, vol. 7, no. 1, pp. 82–85, Feb. 2018.

[12] L. M. Schalk and M. Herrmann, "Suitability of LTE for drone-to-infrastructure communications in very low level airspace," in *Proc. IEEE/AIAA 36th Digit. Avionics Syst. Conf. (DASC)*, St. Petersburg, FL, USA, Sep. 2017, pp. 1–7.

[13] D. W. Matolak and R. Sun, "Air–ground channel characterization for unmanned aircraft systems—Part III: The suburban and near-urban environments," *IEEE Trans. Veh. Technol.*, vol. 66, no. 8, pp. 6607–6618, Aug. 2017.

[14] W. Shi *et al.*, "Multiple drone-cell deployment analyses and optimization in drone assisted radio access networks," *IEEE Access*, vol. 6, pp. 12518–12529, 2018.

[15] Y. Shi, R. Enami, J. Wensowitch, and J. Camp, "Measurement-based characterization of LOS and NLOS drone-to-ground channels," in *Proc. IEEE Wireless Commun. Netw. Conf. (WCNC)*, Barcelona, Spain, Apr. 2018, pp. 1–6.

[16] A. Fotouhi, M. Ding, and M. Hassan. (2017). "DroneCells: Improving 5G spectral efficiency using drone-mounted flying base stations." [Online]. Available: http://arxiv.org/abs/1707.02041

[17] e-CFR. (2018). Title 14: Aeronautics and space—PART 107-small unmanned aircraft systems federal aviation administration. Dept. Transp., Office Federal Register, USA. [Online]. Available: https://www.ecfr.gov/cgi-bin/text-idx?SID=e331c2fe611df1717386d29eee38b000&mc=true&node=pt14.2.107&rgn=div5

[18] A. Al-Hourani, S. Kandeepan, and A. Jamalipour, "Modeling air-to-ground path loss for low altitude platforms in urban environments," in *Proc. IEEE Global Commun. Conf.*, Austin, TX, USA, Dec. 2014, pp. 2898–2904.

[19] A. Fotouhi, M. Ding, and M. Hassan, "Flying drone base stations for macro hotspots," *IEEE Access*, vol. 6, pp. 19530–19539, 2018.

[20] R. Sowah, M. A. Acquah, A. R. Ofoli, G. A. Mills, and K. M. Koumadi, "Rotational energy harvesting to prolong flight duration of quadcopters," *IEEE Trans. Ind. Appl.*, vol. 53, no. 5, pp. 4965–4972, Sep./Oct. 2017.

[21] C. G. L. Krishna and R. R. Murphy, "A review on cybersecurity vulnerabilities for unmanned aerial vehicles," in *Proc. IEEE Int. Symp. Saf., Secur. Rescue Robot. (SSRR)*, Shanghai, China, Oct. 2017, pp. 194–199.

[22] Y.-M. Kwon, J. Yu, B.-M. Cho, Y. Eun, and K.-J. Park, "Empirical analysis of MAVLink protocol vulnerability for attacking unmanned aerial vehicles," *IEEE Access*, vol. 6, pp. 43203–43212, 2018.

[23] J. H. Cheon *et al.*, "Toward a secure drone system: Flying with real-time homomorphic authenticated encryption," *IEEE Access*, vol. 6, pp. 24325–24339, 2018.

[24] M. Lu, M. Bagheri, A. P. James, and T. Phung, "Wireless charging techniques for UAVs: A review, reconceptualization, and extension," *IEEE Access*, vol. 6, pp. 29865–29884, 2018.

[25] H. G. Schantz, "Bottom fed planar elliptical UWB antennas," in *Proc. IEEE Conf. Ultra Wideband Syst. Technol.*, Reston, VA, USA, Nov. 2003, pp. 219–223.

[26] H. G. Schantz, "Apparatus for establishing signal coupling between a signal line and an antenna structure," U.S. Patent 6 512 488, Jan. 28, 2003.

[27] S. R. Saunders and A. Aragón-Zavala, "Antenna parameters," in *Antennas and Propagation for Wireless Communication Systems*, 2nd ed. W. Sussex, Ed. London, U.K.: Wiley, 2007, p. 71.

[28] *System Analysis Module User's Manual PulsON210 UWB Reference Design*, document P210-320-0102B, Time Domain Corporation, Cambridge, MA, USA, Aug. 2005.

[29] Huawei Technologies Co., Ltd. Shenzhen, China, *5G Spectrum Public Policy Position*. Accessed: 2017. [Online]. Available: https://www-file.huawei.com/-/media/CORPORATE/PDF/public-policy/public_policy_position_5g_spectrum.pdf?la=en

[30] P. A. Catherwood and J. McLaughlin, "Internet of Things-enabled hospital wards: Ultrawideband doctor-patient radio channels," *IEEE Antennas Propag. Mag.*, vol. 60, no. 3, pp. 10–18, Jun. 2018.

[31] R. H. Clarke, "Statistical theory of mobile-radio reception," *Bell Syst. Tech. J.*, vol. 47, pp. 957–1000, Jul. 1968.

[32] J. D. Parsons and M. F. Ibrahim, "Signal strength prediction in built-up areas. Part 2: Signal variability," *IEE Proc. F Commun., Radar Signal Process.*, vol. 130, no. 5, pp. 385–391, Aug. 1983.

[33] T. S. Rappaport, "Mobile radiop propagation: Small scale fading and multipath," in *Wireless Communications: Principle and Practice*, 2nd ed. Upper Saddle River, NJ, USA: Prentice-Hall, 2001, p. 147.

[34] J. Liu, M. Ghavami, X. Chu, B. Allen, and W. Malik, "Diversity analysis of multi-antenna UWB impulse radio systems with correlated propagation channels," in *Proc. IEEE Wireless Comms. Netw. Conf. (WCNC)*, Kowloon, China, Mar. 2007, pp. 1593–1598.

[35] T. Kaiser, F. Zheng, and E. Dimitrov, "An overview of ultra-wide-band systems with MIMO," *Proc. IEEE*, vol. 97, no. 2, pp. 285–312, Feb. 2009.

[36] K. P. Burnham and D. R. Anderson, "Information and likelihood theory: a basis for model selection and inference," in *Model Selection and Multimodel Inference: A Practical Information-Theoretic Approach*, 2nd ed. New York, NY, USA: Springer-Verlag, 2011, pp. 60–64.

[37] S. R. Saunders and A. Aragón-Zavala, "Narrowband fast fading," in *Antennas and Propagation for Wireless Communication Systems*, 2nd ed. W. Sussex, Ed. London, U.K.: Wiley, 2007, p. 221.

[38] T. Eltoft, "The Rician inverse Gaussian distribution: A new model for non-Rayleigh signal amplitude statistics," *IEEE Trans. Image Process.*, vol. 14, no. 11, pp. 1722–1735, Nov. 2005.

[39] A. M. Hayajneh, S. A. R. Zaidi, D. C. McLernon, and M. Ghogho, "Optimal dimensioning and performance analysis of drone-based wireless communications," in *Proc. IEEE Globecom Workshops*, Washington, DC, USA, Dec. 2016, pp. 1–6.

[40] J. B. Andersen, T. S. Rappaport, and S. Yoshida, "Propagation measurements and models for wireless communications channels," *IEEE Commun. Mag.*, vol. 33, no. 1, pp. 42–49, Jan. 1995.

[41] A. F. Molisch and M. Steinbauer, "Condensed parameters for characterizing wideband mobile radio channels," *Int. J. Wireless Inf. Netw.*, vol. 6, no. 3, pp. 133–154, Jul. 1999.

[42] S. J. Howard and K. Pahlavan, "Fading results from narrowband measurements of the indoor radio channel," in *Proc. IEEE Int. Symp. Pers., Indoor, Mobile Radio Commun.*, London, U.K., Sep. 1991, pp. 92–97.

[43] N. C. Sagias, G. K. Karagiannidis, D. A. Zogas, P. T. Mathiopoulos, and G. S. Tombras, "Performance analysis of dual selection diversity in correlated Weibull fading channels," *IEEE Trans. Commun.*, vol. 52, no. 7, pp. 1063–1067, Jul. 2004.

[44] A. Al-Hourani, S. Kandeepan, and S. Lardner, "Optimal LAP altitude for maximum coverage," *IEEE Wireless Commun. Lett.*, vol. 3, no. 6, pp. 569–572, Dec. 2014.

[45] M.-S. Alouini and M. K. Simon, "Dual diversity over log-normal fading channels," in *Proc. IEEE Int. Conf. Commun.*, Helsinki, Finland, Jun. 2001, pp. 1089–1093.

EBRAHIM BEDEER MOHAMED received the B.Sc. (Hons.) and M.Sc. degrees in electrical engineering from Tanta University, Tanta, Egypt, and the Ph.D. degree in electrical engineering from Memorial University, St. Johns, NL, Canada. He was a Post-Doctoral Fellow with The University of British Columbia, BC, Canada, and Carleton University, Ottawa, ON, Canada. He is currently an Assistant Professor (Lecturer U.K.) with Ulster University, Jordanstown Campus, U.K. His general research interests are in wireless communications and signal processing, with current focus on the applications of optimization techniques in signal processing and designing Internet of Things-based solutions for disaster management.

He is an Editor of IEEE Communications Letters and the IEEE Access. He served on the technical program committees of numerous major international communication conferences, such as the IEEE GLOBECOM, the IEEE ICC, and the IEEE VTC. He received numerous awards, including the Exemplary Reviewer of the IEEE Communications Letters and the IEEE Wireless Communications Letters.

ADNAN AHMAD CHEEMA received the Ph.D. degree in electronics engineering from Durham University, U.K., in 2015. He continued to work in Durham as a Research Associate on a project funded by OFCOM, U.K., dealing with fifth-generation (5G) radio propagation channel measurements and modeling. In 2017, he joined Ulster University, U.K., as a Lecturer in electronics engineering.

His research interests include drone communications, radio propagation, and the Internet of Things, particularly for applications in 5G, disaster management, and e-health.

JOSEPH RAFFERTY (M'14) received the B.Eng. degree in computer science from Queen's University Belfast, and the M.Sc. degree in computing and the Ph.D. degree in computer science from Ulster University. He is currently a Lecturer with the School of Computing, Ulster University. His research interests include intention recognition, smart environments, agent-based systems, connected health, sensor technology, and planning and intelligent systems.

JAMES A. D. MCLAUGHLIN is a Physicist. He is currently the Head of the School of Engineering, at Ulster University and the Director of NIBEC at Ulster University. His present research interests address point-of-care sensors and medical diagnostics and he has led key developments in sensor materials technology. He is a fellow of the Institute of Physics and the Irish Academy of Engineering. He received the OBE for his services to research and economic development in Northern Ireland.

In recent years, his over-arching strategy is aimed at developing a strong connected health platform with Ulster University. He is the Co-Founder of Intelesens Ltd., which specializes in the design and fabrication of wireless vital-signs monitoring systems, as well as incorporating new micro- and nano-scale technologies, thus enabling the miniaturization and integration of low-cost medical device systems. He has authored or co-authored over 300 publications and holds numerous successful patents. He received outstanding paper awards at international conferences, as well as being honored as an invited keynote speaker at numerous international conferences. He has attracted over £41m of funding to conduct research that has led to the establishment of multiple research centers.

PHILIP A. CATHERWOOD received the B.Eng. degree (Hons.) in engineering and the M.Sc. degree in electronics from the University of Ulster, U.K., in 1997 and 2001, respectively, and the Ph.D. degree in electrical and electronic engineering from the Queen's University of Belfast, U.K., in 2011. He was with the industry for over 10 years developing bespoke scientific measurement equipment and high-speed optical communication devices.

His research explores the Internet of Things networks, wearable wireless medical devices, novel and emerging network technologies, and indoor radio channel modeling. His technical contribution to the telecoms industry was acknowledged through two prestigious industrial recognition awards.

BRENDAN BLACK was born in Belfast, Northern Ireland, in 1994. He received the B.Eng. degree in electronic engineering from Ulster University, in 2017, where he is currently pursuing the Ph.D. degree, with a focus on alternative wireless communication methods for connected health. He has previously been instrumental in the creation and validation of LPWAN solutions for remote healthcare devices.